Selenophene-Based Hole-Transporting Materials for Perovskite Solar Cells

Luis A. Illicachi,[a, b] Javier Urieta-Mora,[c, d] Cristina Momblona,[e] Agustín Molina-Ontoria,*[c] Joaquín Calbo,[f] Juan Aragó,[f] Braulio Insuasty,[a, b] Alejandro Ortiz,[a, b] Enrique Ortí,*[f] Nazario Martín,*[c, d] and Mohammad Khaja Nazeeruddin*[e]

Two novel and simple donor-π-bridge-donor (D-π-D) hole-transporting materials (HTMs) containing two units of the *p*-methoxytriphenylamine (TPA) electron donor group covalently bridged by means of the 3,4-dimethoxyselenophene spacer through single and triple bonds are reported. The optoelectronic and thermal properties of the new selenium-containing HTMs have been determined using standard experimental techniques and theoretical density functional theory (DFT) calculations. The selenium-based HTMs have been incorporated in mesoporous perovskite solar cells (PSCs) in combination with the triple-cation perovskite $[(FAPbI_3)_{0.87}(MAPbBr_3)_{0.13}]_{0.92}[CsPbI_3]_{0.08}$. Limited values of power conversion efficiencies, up to 13.4%, in comparison with the archetype spiro-OMeTAD (17.8%), were obtained. The reduced efficiencies showed by the new HTMs are attributed to their poor film-forming ability, which constrains their photovoltaic performance due to the appearance of structural defects (pinholes).

Introduction

Perovskite solar cells (PSCs) have attracted the attention of the scientific community since the seminal work by Miyasaka,[1] undergoing a continuous growth from the initial 3.8% of power conversion efficiency (PCE) to the recent certified 25.5%.[2,3] The organic-inorganic metal-halide perovskites used in this context present the general formula ABX_3, mixing a small organic cation such as methylammonium (MA^+) or formamidinium (FA^+), a metallic cation (Pb^{2+} or Sn^{2+}), and halides as anions (Br^- or I^-). The combination of different cations and/or anions enables the formation of different compositionally engineered perovskites such as $[FAPbI_3]_{0.85}[MAPbBr_3]_{0.15}$ or $[(FAPbI_3)_{0.87}(MAPbBr_3)_{0.13}]_{0.92}[CsPbI_3]_{0.08}$ that surpass the photovoltaic outcome compared with the standard perovskite $MAPbI_3$.[4,5] Perovskite materials exhibit outstanding optoelectronic properties, namely wide light absorption, high charge-carrier mobilities, tunable bandgap energy, and long charge-carrier diffusion lengths, but also solution processing and high flexibility.[6–8] However, PSCs still suffer from stability issues. Among the possible strategies to overcome this issue, great advances have been reported in the perovskite composition, control of the grain sizes,[9] device encapsulation, interface engineering, and use of protective hole-transporting materials (HTMs) and electron-transporting materials (ETMs).[10–12]

Although the perovskite material can be sandwiched between *n*-type and *p*-type charge selective layers due to its ambipolar behavior, the most widely used PSC architecture employs a mesoporous scaffold of TiO_2, in which the perovskite is infiltrated and covered with an HTM.[13,14] The most commonly used HTM is the well-known 2,2′,7,7′-tetrakis-(*N*,*N*-di-*p*-methoxyphenylamine)-9,9′-spirobifluorene (spiro-OMeTAD) which, despite its excellent photovoltaic performance, requires tedious synthetic and purification steps, thus reducing its potential for low-cost and large-scale photovoltaic applications.[15] In recent years, a wide number of alternative HTMs has been proposed to replace the benchmark spiro-OMeTAD going from inorganic materials (CuSCN, CuO, or NiO)[16–18] to polymers.[19,20] Nevertheless, the most featured HTMs are based on small organic molecules, which can be precisely tuned to maximize their optoelectronic properties through the chemical versatility that characterizes organic materials. Along these lines, HTMs involv-

[a] Dr. L. A. Illicachi, Prof. B. Insuasty, Prof. A. Ortiz
Grupo de Investigación en Compuestos Heterocíclicos, Departamento de Química
Universidad del Valle
Calle 13 No. 100-00, Edificio E20, Cali (Colombia)
[b] Dr. L. A. Illicachi, Prof. B. Insuasty, Prof. A. Ortiz
Center for Research and Innovation in Bioinformatics and Photonics-CIBioFi
Universidad del Valle
Calle 13 No. 100-00, Edificio E20, Cali (Colombia)
[c] Dr. J. Urieta-Mora, Dr. A. Molina-Ontoria, Prof. N. Martín
Departamento Química Orgánica, Facultad C. C. Químicas
Universidad Complutense de Madrid
Av. Complutense s/n, 28040 Madrid (Spain)
E-mail: amolinao@ucm.es
nazmar@ucm.es
Homepage: http://www.nazariomartingroup.com
[d] Dr. J. Urieta-Mora, Prof. N. Martín
IMDEA-Nanociencia
C/Faraday 9, Ciudad Universitaria de Cantoblanco, 28049 Madrid (Spain)
E-mail: nazmar@ucm.es
[e] Dr. C. Momblona, Prof. M. K. Nazeeruddin
Group for Molecular Engineering of Functional Materials
EPFL VALAIS
CH-1951 Sion (Switzerland)
E-mail: mdkhaja.nazeeruddin@epfl.ch
[f] Dr. J. Calbo, Dr. J. Aragó, Prof. Dr. E. Ortí
Instituto de Ciencia Molecular
Universidad de Valencia
46980 Paterna (Spain)
E-mail: enrique.orti@uv.es

Supporting information for this article is available on the WWW under https://doi.org/10.1002/cplu.202100208

This article is part of a Special Collection on "Perovskite Materials and Devices"

ing spiro-containing cores,[21–23] planar heteroaromatic scaffolds,[24–29] or donor-acceptor moieties[30–33] have been synthesized leading to highly efficient PSCs.

Focusing on heteroaromatic cores, selenophene-based materials have been scarcely explored despite the excellent properties that these materials exhibit for optoelectronic applications. Selenium is more polarizable than sulfur, which might induce more effective intermolecular Se-Se interactions leading to an enhanced mobility that is desirable to achieve high photocurrent.[34–36] Selenophene is indeed an important building block in technological applications such as organic light-emitting diodes (OLEDs),[37] organic field-effect transistors (OFETs),[38] organic solar cells (OSCs),[39] and perovskite solar cells (PSCs).[40] Herein, we present the synthesis and characterization of two novel donor-π-bridge-donor (D-π-D) selenophene-based HTMs, named **TPASe-1** and **TPASe-2**, where a methoxy-substituted selenophene moiety is used as π-conjugated linker between two electron-donor *p*-methoxytriphenylamine (TPA) units through single and triple bonds, respectively. The two new HTMs have been tested in mesoporous PSCs in combination with the triple-cation perovskite $[(FAPbI_3)_{0.87}(MAPbBr_3)_{0.13}]_{0.92}[CsPbI_3]_{0.08}$, and the photovoltaic performance of the resulting solar cells has been evaluated. A detailed study of the optical, electrochemical, and thermal properties of **TPASe-1** and **TPASe-2**, assisted by density functional theory (DFT) calculations, is also provided.

Results and Discussion

Synthesis of TPASe HTMs

The synthetic route used for the preparation of the **TPASe-1** and **TPASe-2** HTMs is illustrated in Scheme 1 and the experimental conditions are detailed in the Supporting Information (SI). The synthesis of the central scaffold of 2,5-dibromo-3,4-dimethoxyselenophene (**3**) was conducted following a well-established procedure.[41] First, an "in situ" prepared solution of $SeCl_2$ solution was reacted with 2,3-dimethoxy-1,3-butadiene in the presence of sodium acetate affording 3,4-dimethoxyselenophene (**2**). Then, compound **2** was regioselectively brominated in the α-positions using *N*-bromosuccinimide (NBS) at 0 °C affording the dibrominated compound **3**. Subsequently, a two-fold Suzuki cross-coupling reaction with 4-methoxy-*N*-(4-(4,4,5,5-tetramethyl-1,3,2-dioxaborolan-2-yl)phenyl)aniline successfully furnished **TPASe-1** in moderate yield (44%). Likewise, **TPASe-2** was synthesized through a two-fold Sonogashira cross-coupling reaction between compound **3** and 4-ethynyl-*N*,*N*-bis(4-methoxyphenyl)aniline in moderate yield (48%). A complete structural characterization of the aforementioned HTMs was carried out using ^{1}H NMR, ^{13}C NMR, FT-IR, and UV-Vis absorption and emission spectroscopic techniques. The proposed structures were determined by mass spectrometry (see the Supporting Information (SI)).

Structural, (opto)electronic, and thermal properties of TPASe-1 and TPASe-2

Theoretical calculations were performed using the density functional theory (DFT) framework to shed light on the structural and electronic properties of the selenophene-based **TPASe-1** and **TPASe-2** HTMs. Minimum-energy structures were obtained after full geometry optimization at the B3LYP/6-31G (d,p) level of theory using tetrahydrofuran (THF) as solvent (see the SI for computational details). **TPASe-1** displays a quasi-coplanar D-π-D structure, with dihedral angles of ~27° between the selenophene ring and the adjacent benzene of each TPA unit (Figure S1). In contrast, the presence of triple bonds between the selenophene moiety and the TPA units allows for a coplanar arrangement of the central conjugated core in **TPASe-2** (Figure S1). In both derivatives, the TPA moieties show the typical propeller configuration due to the evident steric hindrance between the phenyl rings.

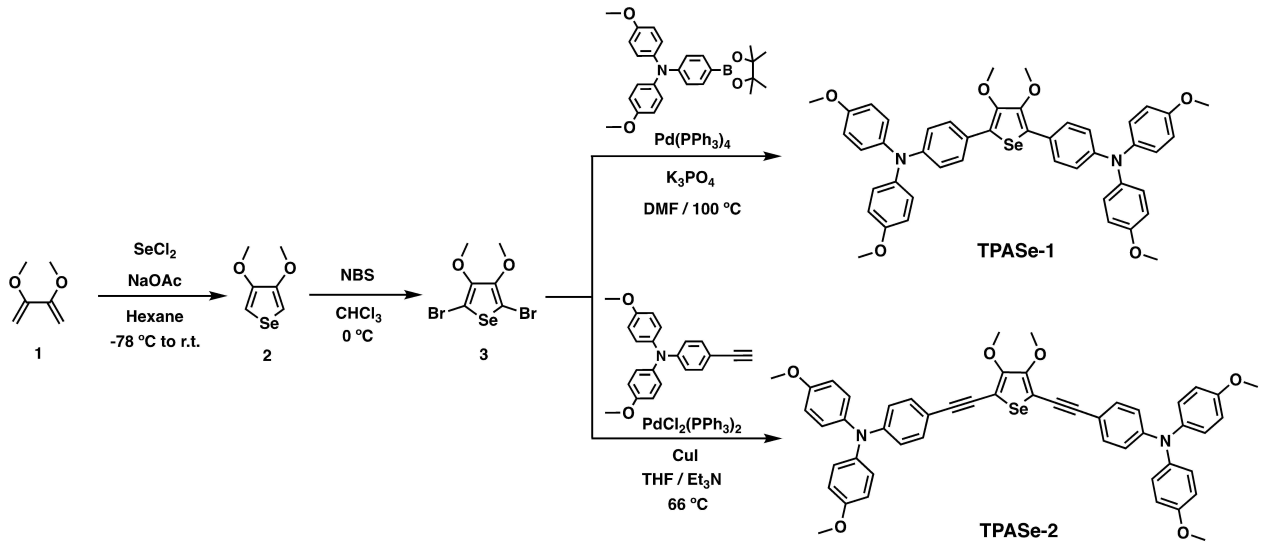

Scheme 1. Synthetic approach for the preparation of **TPASe-1** and **TPASe-2**.

The frontier molecular orbitals calculated at the B3LYP/6-31G(d,p) level indicate that the highest-occupied molecular orbital (HOMO) spreads all over the molecular structure for both derivatives, whereas the HOMO-1 is centered on the TPA units (Figure 1a). In addition, the lowest-unoccupied molecular orbital (LUMO) is localized over the central part of the molecule, including the selenophene and the contiguous benzene rings of the TPAs. These results indicate that the TPA units are highly conjugated along the selenophene π-bridge and, therefore, the electronic nature of the molecular fragments constituting the TPA-selenophene-TPA structure is mixed. The HOMO for **TPASe-1** and **TPASe-2** is calculated at −4.54 and −4.59 eV, respectively, supporting that **TPASe-1** is a stronger electron donor than **TPASe-2**. On the other hand, the LUMO of **TPASe-2** is computed at −1.76 eV, lower in energy than that of **TPASe-1** (−1.34 eV), pointing to an easier tendency for **TPASe-2** to be reduced. The HOMO-LUMO energy gap is therefore predicted to be 3.20 and 2.83 eV for **TPASe-1** and **TPASe-2**, respectively, suggesting a lower energy HOMO→LUMO transition in **TPASe-2**.

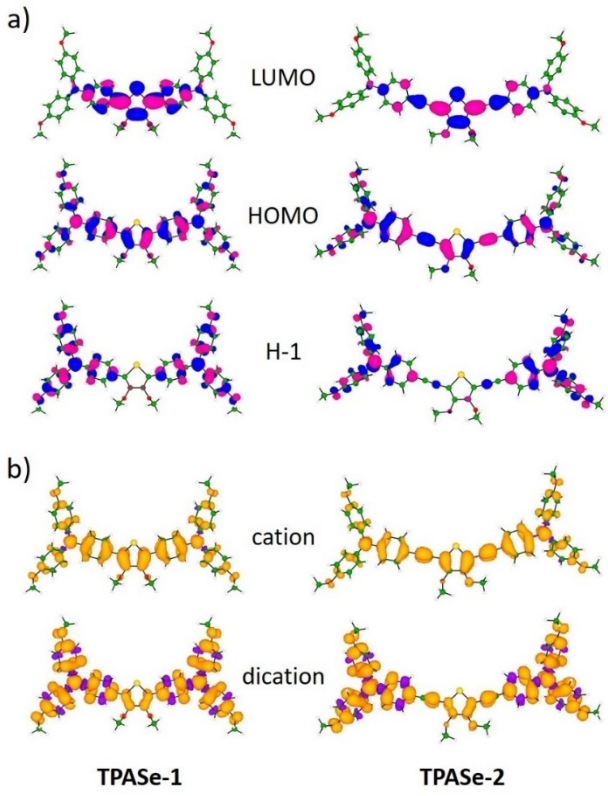

Figure 1. (a) Frontier molecular orbital contours (isovalue = 0.03) and (b) spin densities upon one (cation) and two-electron (dication) extractions (isovalue = 0.001) calculated at the B3LYP/6-31G(d,p) level for **TPASe-1** and **TPASe-2**.

The optical properties of **TPASe-1** and **TPASe-2** were investigated by recording the UV-Vis absorption and emission spectra in solution (THF) as shown in Figure 2a. The maximum absorption and emission wavelengths are listed in Table 1. The UV-Vis absorption spectra show maximum absorption bands for the novel **TPASe-1** and **TPASe-2** HTMs centered at 402 and 407 nm, respectively. As discussed above on the basis of theoretical calculations, the broader and slightly red-shifted absorption of **TPASe-2** compared with **TPASe-1** is attributed to the more extended π-conjugation obtained by linking the TPA units with the central 3,4-dimethoxyselenophene group through triple bonds.[42] On the other hand, the emission spectra display broad bands with maximum emission bands centered at 513 and 508 nm for **TPASe-1** and **TPASe-2**, respectively. The optical band gap ($E^{0\text{-}0}$), estimated from the intersection of the absorption and emission bands, resulted in values of 2.77 and 2.72 eV for **TPASe-1** and **TPASe-2**, respectively, which are significantly lower than that reported for the reference compound spiro-OMeTAD (3.05 eV).

Time-dependent DFT calculations at the B3LYP/6-31G(d,p) level in THF confirm the presence of an intense, low-lying, singlet excited state S_1 described by the HOMO→LUMO monoexcitation in our selenophene-based HTMs (Figure S3). The electronic transition to S_1 is predicted at lower energies for **TPASe-2** (2.51 eV; 494 nm) than for **TPASe-1** (2.76 eV; 450 nm), in good accord with the HOMO-LUMO gap trends, and supporting the red-shift experimentally recorded upon extending the π-conjugated bridge with the triple bonds.[44]

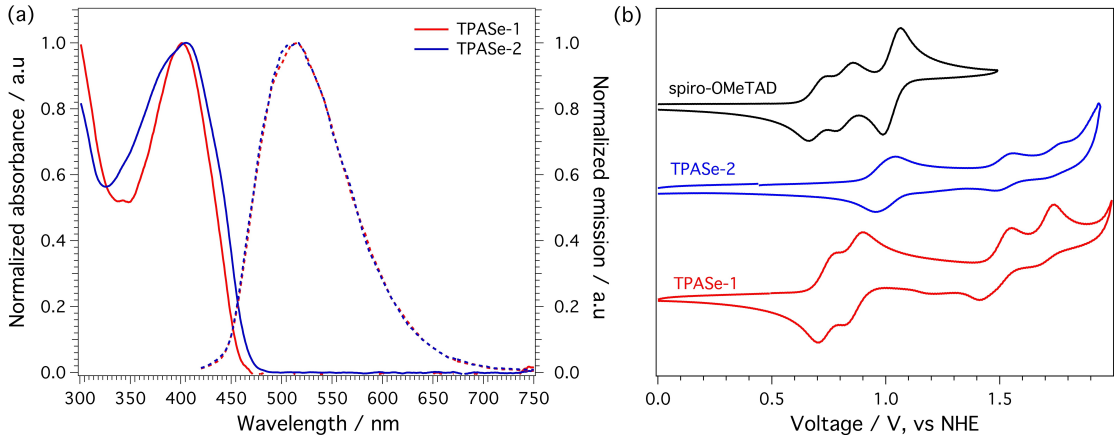

Figure 2. (a) UV-Vis absorption spectra (solid line) and fluorescence emission spectra (dashed line) recorded for **TPASe-1** and **TPASe-2** in THF. (b) Cyclic voltammetry of **TPASe-1** and **TPASe-2** in THF solution containing 0.1 M $TBAPF_6$ measured at a scan rate of 100 mV s^{-1}.

Table 1. Optical, electrochemical, and thermal properties of **TPASe-1**, **TPASe-2**, and spiro-OMeTAD.

HTM	$\lambda_{max,\ abs}$ [nm][a]	$\lambda_{max,\ em}$ [nm][a]	$E_{0\text{-}0}$ [eV][b]	$E_{ox1/2}$ [V][c]	E_{HOMO} [eV][d]	E_{LUMO} [eV][e]	T_{dec} [°C][f]	T_g [°C][g]
TPASe-1	402	513	2.77	0.74	−5.18	−2.41	348	81
TPASe-2	407	508	2.72	0.99	−5.43	−2.71	327	72
spiro-OMeTAD[43]	385	419	3.05	0.72	−5.16	−2.11	449	125

[a] λ_{max} of absorption and emission measured in THF solutions. [b] E^{0-0} was determined at the intersection of normalized absorption and emission spectra. [c] Determined from cyclic voltammetry measurements *vs* normal hydrogen electrode (NHE). [d] E_{HOMO} is calculated by $E_{HOMO} = -4.44\ eV - E^{ox}_{1/2}$. [e] E_{LUMO} was estimated by $E_{LUMO} = E_{HOMO} + E^{0-0}$. [f] Decomposition temperature determined from TGA (5% weight loss under a N_2 atmosphere). [g] Determined from the first cycle of the DSC under a N_2 atmosphere.

The electrochemical properties of the new HTMs were studied by cyclic voltammetry (CV) in $TBAPF_6$/THF at a scan rate of 100 $mV\,s^{-1}$ as depicted in Figure 2b, and the corresponding redox potentials are gathered in Table 1. The selenophene-containing HTMs are active in the anodic region, but their electrochemical behavior is significantly different. **TPASe-1** exhibits four oxidation waves at half-wave potentials ($E^{ox}_{1/2}$) of 0.74, 0.86, 1.51, and 1.71 eV *vs* normal hydrogen electrode (NHE). The first two oxidations can be tentatively assigned to the extraction of two consecutive electrons from the donor TPA units. The HOMO energy estimated for **TPASe-1** from the first oxidation potential is calculated at −5.18 eV, a value almost identical to that obtained for the benchmark spiro-OMeTAD (−5.16 eV). On the other hand, **TPASe-2** exhibits three oxidation waves, the first one showing a higher intensity being assigned to the simultaneous extraction of two electrons from the TPA units. The first $E^{ox}_{1/2}$ of **TPASe-2** is located at 0.99 V (HOMO energy of −5.43 eV), which indicates a weaker electron-donor ability compared to **TPASe-1**. An efficient hole extraction from the perovskite to the HTM is expected due to the excellent band alignment of the HOMO of the new HTMs with the valence band edge of the triple-cation $[(FAPbI_3)_{0.87}(MAPbBr_3)_{0.13}]_{0.92}[CsPbI_3]_{0.08}$ perovskite (*ca.* −5.7 eV).

Theoretical calculations were performed on the charged species of **TPASe-1** and **TPASe-2** to fully rationalize the electron extraction processes taking place upon oxidation. In contrast to that initially hypothesized, the first electron extraction occurs from both the bridging core and the TPA moieties, as evidenced by the unpaired-electron spin density contours calculated for the cation species (Figure 1b). The Mulliken atomic charges accumulated by the molecular fragments confirm this picture, with 0.50e extracted from the conjugated central part of the molecule (including selenophene and vicinal benzenes) and 0.50e from the DPAs (TPAs excluding the inner benzene ring) in **TPASe-1** (Table S2). Similarly, the electron extraction upon first oxidation of **TPASe-2** is predicted to be 0.58e from the central core and 0.42e from the DPAs. The theoretical first ionization energy (IE) is calculated to be 4.45 and 4.52 eV for **TPASe-1** and **TPASe-2**, respectively, supporting the stronger electron-donor character of the former. On the other hand, the second oxidation is predicted to occur mainly on the external DPA units, as evidenced by the spin density and the atomic charges (Figure 1b and Table S2). The second IE is calculated very similar for both HTMs, at 5.07 and 5.01 eV for **TPASe-1** and **TPASe-2**, respectively, as expected from the TPA-centered nature of this oxidation process. The second oxidation is indeed associated with the extraction of an electron from the HOMO-1, which is fully located on the TPA units for both HTMs (Figure 1a), and gives rise to an open-shell triplet dication. The energy difference between the first and the second IE is calculated smaller than 0.5 eV for **TPASe-1** (0.49 eV), whereas it is larger than 0.5 eV for **TPASe-2** (0.62 eV), which supports the single wave and the double wave recorded respectively for the two first oxidation features in the CV experiments for **TPASe-1** and **TPASe-2**, respectively. Finally, the third and fourth oxidation processes imply the whole molecule and the DPAs, respectively (Figure S4 and Table S2), with differences between consecutive IEs greater than 0.6 eV (Table S3).

To evaluate the thermal properties of the new HTMs, thermogravimetric analysis (TGA) and differential scanning calorimetry (DSC) experiments were performed under nitrogen atmosphere (Figure 3), the detailed thermal features being listed in Table 1. From TGA analyses, both HTMs exhibit good thermal stability with decomposition temperatures (T_{dec}) of 348 and 327 °C (5% weight loss under a N_2 atmosphere) for **TPASe-1** and **TPASe-2**, respectively. However, these values are significantly lower than that measured for the state-of-the-art spiro-OMeTAD (449 °C). The relatively lower T_{dec} observed for **TPASe-1** and **TPASe-2** in comparison to the benchmark spiro-OMeTAD are attributed to the more rigid structure of spiro-OMeTAD. To gain further insight into the thermal behavior of the selenophene-containing HTMs, DSC experiments were carried out (Figure 3b). Both derivatives can exist in both crystalline and amorphous states showing low glass transition temperatures (T_g) detected at 81 °C and 72 °C for **TPASe-1** and **TPASe-2**, respectively, during the first cycle. In comparison, spiro-OMeTAD show a similar thermal behavior but with a higher T_g of 125 °C, which should be beneficial for the photovoltaic performance as HTM in PSCs under operational conditions.

Photovoltaic properties of TPASe HTMs

The photovoltaic performance of the selenophene-containing HTMs was evaluated in solution-processed PSCs and compared with spiro-OMeTAD as reference. The PSC devices were prepared in an *n-i-p* mesoporous configuration with the architecture FTO/c-TiO_2 (30 nm)/mp-TiO_2 (250 nm)/SnO_2/Perovskite (400 nm)/HTM (100–110 nm)/Au (80 nm), and using as

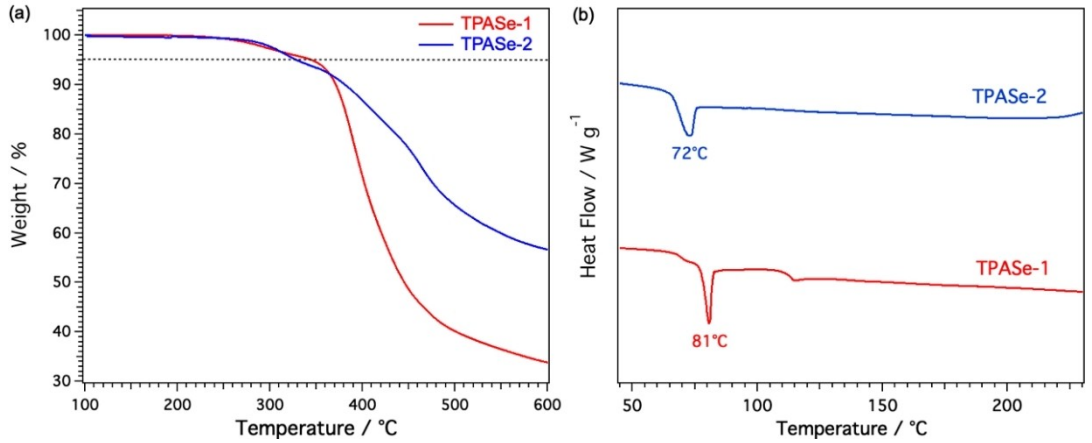

Figure 3. (a) Thermogravimetric analysis curves recorded under nitrogen atmosphere at 10 °C min^{-1} of heating rate. (b) Differential scanning calorimetry curves under nitrogen atmosphere at a heating rate of 20 °C min^{-1} (first cycle).

light-harvesting material the widely employed triple-cation perovskite $[(FAPbI_3)_{0.87}(MAPbBr_3)_{0.13}]_{0.92}[CsPbI_3]_{0.08}$. The HTMs were deposited by spin-coating a chlorobenzene solution with an optimized concentration of 20 mM. Both HTMs were chemically doped with standard tris(2-(1*H*-pyrazol-1-yl)-4-*tert*-butylpyridine)cobalt(III) tri[bis(trifluoromethane)sulfonimide] (FK-209), bis(trifluoromethane)sulfonimide lithium salt (LiTFSI), and *tert*-butylpyridine (^{t}BP) as additives. The detailed device fabrication is outlined in the Supporting Information. Figure 4a shows the schematic illustration of the energy levels of the different constituents of the PSC. Both HTMs exhibit a good band alignment with their HOMO energy above the valence band edge of the triple-cation perovskite, thus facilitating the hole extraction from the perovskite and blocking the electron extraction due to their high LUMO energy. The cross-section scanning electron microscopy (SEM) images of the devices are illustrated in Figures 4b-c. Despite the excellent solubility of the new HTMs in chlorobenzene, the cross-sectional images show a poor film formation of **TPASe-1** and **TPASe-2**. In both cases, the presence of pinholes is detected, which clearly envisages a detrimental impact on their photovoltaic performance. The formation of these pinholes is also demonstrated in the top view of the SEM images (Figures S5 and S6), particularly for **TPASe-2**.

The photovoltaic performance of the selenophene-based HTMs in solution-processed PSCs was evaluated under simu-

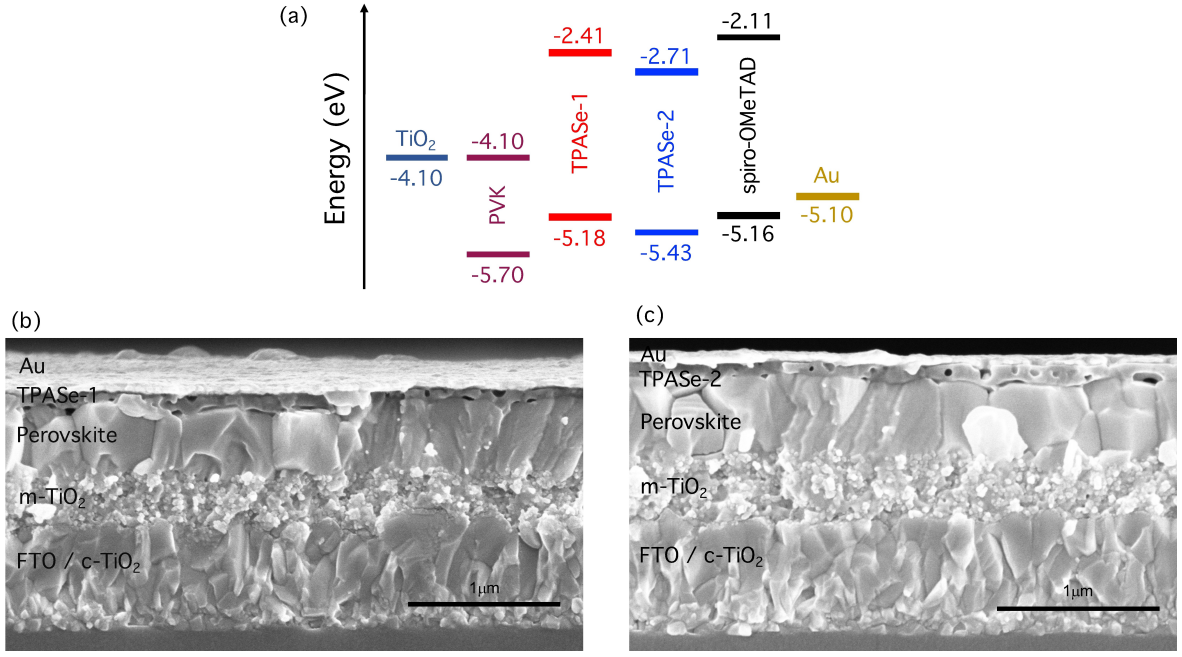

Figure 4. (a) Energy level diagram of the different constituents used in the PSC. Cross-section SEM images of the corresponding mesoporous (FTO/c-TiO_2/mp-TiO_2/SnO_2/Perovskite/HTM/Au) PSC devices fabricated with (b) **TPASe-1** and (c) **TPASe-2**.

lated illumination of 1 sun AM 1.5 G (100 mW cm^{-2}). Figure 5a displays the current density-voltage (*J-V*) for the best-performing PSCs and Table 2 gathers the corresponding photovoltaic parameters. **TPASe-1**-based devices showed the best efficiencies exhibiting a maximum power conversion efficiency (PCE) of 13.72% with an open-circuit voltage (V_{oc}) of 932 mV, a short-circuit current (J_{sc}) of 22.49 mA cm^{-2}, and a field factor (*FF*) of 0.65, showing reduced hysteresis. **TPASe-2**-based devices reached a lower efficiency than those using **TPASe-1**, due to the significant decrease of the V_{oc} (903 mV) that leads to a smaller *FF* (0.61) with an enhanced hysteresis. The low homogeneity and uniformity of the selenium-containing HTM films favors the interfacial charge recombination, which contributes to the low *FF* values obtained for the novel HTMs.[45] The devices incorporating spiro-OMeTAD as HTM surpassed the PCE values provided by the selenophene derivatives, reaching a maximum PCE of 17.78% correlated with the enhanced values of V_{oc} (1056 mV), J_{sc} (23.28 mA cm^{-2}), and *FF* (0.73). Figure 5b displays the external quantum efficiencies (EQEs) of the new selenium-containing HTMs and the reference of spiro-OMeTAD and the integrated photocurrents deduced for **TPASe-1** (22.42 mA cm^{-2}), **TPASe-2** (22.43 mA cm^{-2}), and spiro-OMeTAD (23.34 mA cm^{-2}) are in good agreement with those obtained from the *J-V* measurements.

The charge-transporting behavior of the doped **TPASe-1** and **TPASe-2** was investigated by using the space-charge-limited current (SCLC) method. The hole mobility was estimated to be 6.14×10^{-5} cm^{2}V^{-1}s^{-1} for **TPASe-1** and 7.01×10^{-5} cm^{2}V^{-1}s^{-1} for **TPASe-2** (Figure S7). These mobilities are around 5–6 times lower than that recorded for spiro-OMeTAD

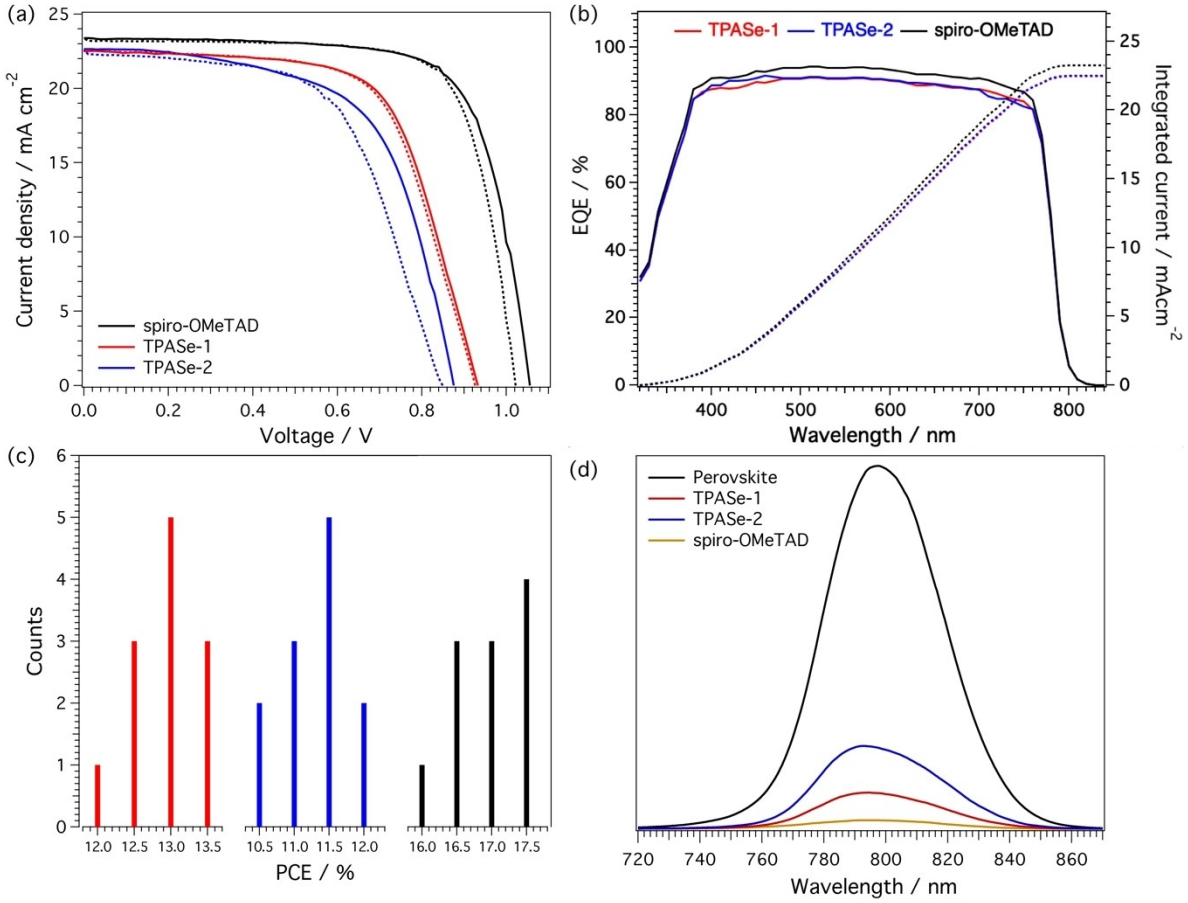

Figure 5. (a) *J-V* curves of **TPASe-1**, **TPASe-2**, and spiro-OMeTAD in combination with the triple-cation $[(FAPbI_3)_{0.87}(MaPbI_3)_{0.13}]_{0.92}[CsPbI_3]_{0.08}$ perovskite in mesoporous PSC devices (forward scan in solid line and reverse scan in dashed line). (b) EQE measurements and the corresponding integrated current for **TPASe-1**, **TPASe-2**, and spiro-OMeTAD. (c) Device stadistics of 12 devices incorporating **TPASe-1**, **TPASe-2**, and spiro-OMeTAD as HTM. (d) Steady-state PL spectra of the pristine triple-cation perovskite and perovskite/HTM films.

Table 2. Photovoltaic parameters of the best performing PSCs containing **TPASe-1**, **TPASe-2**, and spiro-OMeTAD as HTMs. Average values from measurements on 12 devices are given within parentheses.

HTM	V_{oc} [V]	J_{sc} [mA cm^{-2}]	FF	PCE [%]
TPASe-1	0.93 (0.92 ± 0.01)	22.49 (22.50 ± 0.11)	0.65 (0.63 ± 0.02)	13.72 (13.01 ± 0.51)
TPASe-2	0.90 (0.86 ± 0.02)	22.52 (22.55 ± 0.12)	0.61 (0.59 ± 0.02)	12.44 (11.45 ± 0.51)
spiro-OMeTAD	1.06 (1.03 ± 0.02)	23.28 (23.20 ± 0.21)	0.73 (0.71 ± 0.02)	17.78 (17.15 ± 0.53)

(3.71×10^{-4} $cm^2V^{-1}s^{-1}$), which also contributes to the modest performance of **TPASe-1** and **TPASe-2** PSC devices in comparison with spiro-OMeTAD.

To shed light on the hole-extraction capability of the selenophene-based HMTs compared to spiro-OMeTAD, steady-state photoluminescence (PL) spectra were recorded (Figure 5d). Upon excitation, the pristine triple-cation perovskite film shows a strong PL band centered at 785 nm, which is clearly quenched when the HTMs are deposited on top of the perovskite, indicating that the photogenerated holes are efficiently extracted at the perovskite/HTM interface. However, it should be noted that spiro-OMeTAD presents a significantly more efficient hole-extraction behavior than the selenium-containing HTMs, and among the later **TPASe-1** performs better than **TPASe-2**, which is in good agreement with the photovoltaic performance measured in PSCs.

Conclusion

In summary, the design and synthesis of two new hole-transporting materials, **TPASe-1** and **TPASe-2**, using the 3,4-dimethoxyselenophene unit as central scaffold have been described. The new HTMs incorporate two *p*-methoxytriphenylamine TPA donor units, linked through single and triple bonds to the central spacer, and are prepared following straightforward syntheses with relatively good yields. They show highly conjugated, almost planar, donor-π-bridge-donor structures. Both HTMs exhibit strong absorption and emission in the visible region and adequate HOMO alignment (−5.18 eV and −5.43 eV for **TPASe-1** and **TPASe-2**, respectively) with the valence band edge of the triple-cation $[(FAPbI_3)_{0.87}(MAPbBr_3)_{0.13}]_{0.92}[CsPbI_3]_{0.08}$ perovskite (−5.70 eV). The donor-acceptor-donor linker group influences the electrochemical properties of the two new HTMs. The single bonds promote the extraction of two consecutive electrons from the donor TPA units in **TPASe-1**. In comparison, the triple bonds induce the simultaneous extraction of two electrons from the TPA units due to the enhanced conjugation in **TPASe-2**. The selenium-based HTMs were applied in *n-i-p* mesoporous perovskite solar cells using the state-of-the-art $[(FAPbI_3)_{0.87}(MAPbBr_3)_{0.13}]_{0.92}[CsPbI_3]_{0.08}$ as light absorber, reaching moderate efficiencies (13.72 and 12.44% for **TPASe-1** and **TPASe-2**, respectively), lower than those obtained for the reference compound of spiro-OMeTAD (17.78%). The limited performance of the selenium-based HTMs is attributed to the poor film-formation ability of both derivatives on top of the perovskite layer and also to their lower hole mobility in comparison to spiro-OMeTAD. Both HTMs form layers containing pinholes, which have a clear negative impact on the photovoltaic performance. Photoluminescence experiments on perovskite/HTM thin films show that the hole-extraction ability of the HTM decreases in passing from spiro-OMeTAD to **TPASe-1** and to **TPASe-2**, in good agreement with the decrease observed in the PSC performance.

Acknowledgements

We thank the Swiss National Funds for Scientific Research contract number 200020 L 172929/1. The authors also thank the Spanish Ministry of Science and Innovation (MICINN) (projects CTQ2017-83531-R, PGC2018-099568-B–I00, RED2018-102815-T, Centro de Excelencia Severo Ochoa SEV-2016-0686, and Unidad de Excelencia María de Maeztu CEX2019-000919-M), the CAM (QUIMTRONIC-CM project Y2018/NMT-4783), the Generalitat Valenciana (PROMETEO/2020/07), and European Feder funds (PGC2018-099568-B–I00). J.A. and A.M.O. are grateful to MICINN for "Ramon-y-Cajal" fellowships (RyC-2017-23500, RYC2019-027280-I). L.I. thanks to the Universidad del Valle (CIAM-2017) and the Science, Technology and Innovation Fund-General Royalties System (FCTeI-SGR) under contract BPIN 2013000100007 for a predoctoral fellowship. Borun New Material Technology generously supplied the high-quality spiro-OMeTAD.

Conflict of Interest

The authors declare no conflict of interest.

Keywords: donor-bridge-donor systems · hole-transporting materials · perovskite solar cells · photophysics · selenophenes

[1] A. Kojima, K. Teshima, Y. Shirai, T. Miyasaka, *J. Am. Chem. Soc.* **2009**, *131*, 6050–6051.
[2] J. J. Yoo, G. Seo, M. R. Chua, T. G. Park, Y. Lu, F. Rotermund, Y.-K. Kim, C. S. Moon, N. J. Jeon, J.-P. Correa-Baena, V. Bulović, S. S. Shin, M. G. Bawendi, J. Seo, *Nature* **2021**, *590*, 587–593.
[3] N. R. E. L. National Renewable Energy Laboratory, "http://www.nrel.gov/ncpv/images/efficiency chart.jpg, (accessed April 1, 2021).," **2021**.
[4] G. E. Eperon, S. D. Stranks, C. Menelaou, M. B. Johnston, L. M. Herz, H. J. Snaith, *Energy Environ. Sci.* **2014**, *7*, 982–988.
[5] M. Saliba, T. Matsui, J.-Y. Seo, K. Domanski, J.-P. Correa-Baena, M. K. Nazeeruddin, S. M. Zakeeruddin, W. Tress, A. Abate, A. Hagfeldt, M. Gratzel, *Energy Environ. Sci.* **2016**, *9*, 1989–1997.
[6] T. M. Brenner, D. A. Egger, L. Kronik, G. Hodes, D. Cahen, *Nat. Rev. Mater.* **2016**, *1*, 15007.
[7] Y. Zhao, K. Zhu, *Chem. Soc. Rev.* **2016**, *45*, 655–689.
[8] D. Shi, V. Adinolfi, R. Comin, M. Yuan, E. Alarousu, A. Buin, Y. Chen, S. Hoogland, A. Rothenberger, K. Katsiev, Y. Losovyj, X. Zhang, P. A. Dowben, O. F. Mohammed, E. H. Sargent, O. M. Bakr, *Science* **2015**, *347*, 519–522.
[9] W. Xu, G. Lei, C. Tao, J. Zhang, X. Liu, X. Xu, W.-Y. Lai, F. Gao, W. Huang, *Adv. Funct. Mater.* **2018**, *28*, 1802320.
[10] R. Wang, M. Mujahid, Y. Duan, Z.-K. Wang, J. Xue, Y. Yang, *Adv. Funct. Mater.* **2019**, *29*, 1808843.
[11] Z. Yang, B. H. Babu, S. Wu, T. Liu, S. Fang, Z. Xiong, L. Han, W. Chen, *Solar RRL* **2020**, *4*, 1900257.
[12] E. H. Jung, N. J. Jeon, E. Y. Park, C. S. Moon, T. J. Shin, T.-Y. Yang, J. H. Noh, J. Seo, *Nature* **2019**, *567*, 511–515.
[13] J. Urieta-Mora, I. García-Benito, A. Molina-Ontoria, N. Martín, *Chem. Soc. Rev.* **2018**, *47*, 8541–8571.
[14] K. Rakstys, C. Igci, M. K. Nazeeruddin, *Chem. Sci.* **2019**, *10*, 6748–6769.
[15] Z. Hawash, L. K. Ono, Y. Qi, *Adv. Mater. Interfaces* **2018**, *5*, 1700623.
[16] N. Arora, M. I. Dar, A. Hinderhofer, N. Pellet, F. Schreiber, S. M. Zakeeruddin, M. Grätzel, *Science* **2017**, *358*, 768–771.
[17] W. Sun, Y. Li, S. Ye, H. Rao, W. Yan, H. Peng, Y. Li, Z. Liu, S. Wang, Z. Chen, L. Xiao, Z. Bian, C. Huang, *Nanoscale* **2016**, *8*, 10806–10813.
[18] B. Zhang, J. Su, X. Guo, L. Zhou, Z. Lin, L. Feng, J. Zhang, J. Chang, Y. Hao, *Adv. Sci.* **2020**, *7*, 1903044.
[19] X. Sun, Z. Li, X. Yu, X. Wu, C. Zhong, D. Liu, D. Lei, A. K.-Y. Jen, Z. Li, Z. Zhu, *Angew. Chem. Int. Ed.* **2021**, *60*, 7227–7233.

[20] M. J. Jeong, K. M. Yeom, S. J. Kim, E. H. Jung, J. H. Noh, *Energy Environ. Sci.* **2021**, *14*, 2419–2428.
[21] M. Saliba, S. Orlandi, T. Matsui, S. Aghazada, M. Cavazzini, J.-P. Correa-Baena, P. Gao, R. Scopelliti, E. Mosconi, K.-H. Dahmen, F. De Angelis, A. Abate, A. Hagfeldt, G. Pozzi, M. Graetzel, M. K. Nazeeruddin, *Nat. Energy* **2016**, *1*, 15017.
[22] N. J. Jeon, H. Na, E. H. Jung, T.-Y. Yang, Y. G. Lee, G. Kim, H. W. Shin, S. I. Seok, J. Lee, J. Seo, *Nat. Energy* **2018**, *3*, 682–689.
[23] M. Jeong, I. W. Choi, E. M. Go, Y. Cho, M. Kim, B. Lee, S. Jeong, Y. Jo, H. W. Choi, J. Lee, J.-H. Bae, S. K. Kwak, D. S. Kim, C. Yang, *Science* **2020**, *369*, LP 1615–1620.
[24] A. Molina-Ontoria, I. Zimmermann, I. Garcia-Benito, P. Gratia, C. Roldán-Carmona, S. Aghazada, M. Graetzel, M. K. Nazeeruddin, N. Martín, *Angew. Chem. Int. Ed.* **2016**, *55*, 6270–6274; *Angew. Chem.* **2016**, *128*, 6378–6382.
[25] J. Zhou, X. Yin, Z. Dong, A. Ali, Z. Song, N. Shrestha, S. S. Bista, Q. Bao, R. J. Ellingson, Y. Yan, W. Tang, *Angew. Chem. Int. Ed.* **2019**, *58*, 13717–13721; *Angew. Chem.* **2019**, *131*, 13855–13859.
[26] I. Zimmermann, J. Urieta-Mora, P. Gratia, J. Aragó, G. Grancini, A. Molina-Ontoria, E. Ortí, N. Martín, M. K. Nazeeruddin, *Adv. Energy Mater.* **2017**, *7*, 1601674.
[27] J. Urieta-Mora, I. Zimmermann, J. Aragó, A. Molina-Ontoria, E. Ortí, N. Martín, M. K. Nazeeruddin, *Chem. Mater.* **2019**, *31*, 6435–6442.
[28] F. Zhang, Z. Wang, H. Zhu, N. Pellet, J. Luo, C. Yi, X. Liu, H. Liu, S. Wang, X. Li, Y. Xiao, S. M. Zakeeruddin, D. Bi, M. Grätzel, *Nano Energy* **2017**, *41*, 469–475.
[29] X.-C. Li, Y.-G. Tu, C. Meng, W. Song, T. Cheng, Y.-T. Gong, J. Min, R. Zhu, W.-Y. Lai, W. Huang, *ACS Appl. Mater. Interfaces* **2019**, *11*, 45717–45725.
[30] K. Rakstys, S. Paek, P. Gao, P. Gratia, T. Marszalek, G. Grancini, K. T. Cho, K. Genevicius, V. Jankauskas, W. Pisula, M. K. Nazeeruddin, *J. Mater. Chem. A* **2017**, *5*, 7811–7815.
[31] J. A. Christians, P. Schulz, J. S. Tinkham, T. H. Schloemer, S. P. Harvey, B. J. Tremolet de Villers, A. Sellinger, J. J. Berry, J. M. Luther, *Nat. Energy* **2018**, *3*, 68–74.
[32] D. Vaitukaityte, Z. Wang, T. Malinauskas, A. Magomedov, G. Bubniene, V. Jankauskas, V. Getautis, H. J. Snaith, *Adv. Mater.* **2018**, *30*, 1803735.
[33] X.-C. Li, C.-Y. Wang, W.-Y. Lai, W. Huang, *J. Mater. Chem. C* **2016**, *4*, 10574–10587.
[34] R. L. Uy, L. Yan, W. Li, W. You, *Macromolecules* **2014**, *47*, 2289–2295.
[35] A. Patra, Y. H. Wijsboom, S. S. Zade, M. Li, Y. Sheynin, G. Leitus, M. Bendikov, *J. Am. Chem. Soc.* **2008**, *130*, 6734–6736.
[36] Z. Liang, M. Li, X. Zhang, Q. Wang, Y. Jiang, H. Tian, Y. Geng, *J. Mater. Chem. A* **2018**, *6*, 8059–8067.
[37] W. Cho, G. Sarada, H. Lee, M. Song, Y.-S. Gal, Y. Lee, S.-H. Jin, *Dyes Pigm.* **2017**, *136*, 390–397.
[38] B. Kim, H. R. Yeom, M. H. Yun, J. Y. Kim, C. Yang, *Macromolecules* **2012**, *45*, 8658–8664.
[39] D. Meng, D. Sun, C. Zhong, T. Liu, B. Fan, L. Huo, Y. Li, W. Jiang, H. Choi, T. Kim, J. Y. Kim, Y. Sun, Z. Wang, A. J. Heeger, *J. Am. Chem. Soc.* **2016**, *138*, 375–380.
[40] R. K. Gunasekaran, P. J. S. Rana, S. H. Park, V. Tamilavan, S. Karuppanan, H.-J. Kim, K. Prabakar, *Sol. Energy Mater. Sol. Cells* **2019**, *199*, 66–74.
[41] B. Kim, J. Kim, E. Kim, *Macromolecules* **2011**, *44*, 8791–8797.
[42] A. Tigreros, A. Ortiz, B. Insuasty, *Dyes Pigm.* **2014**, *111*, 45–51.
[43] I. García-Benito, I. Zimmermann, J. Urieta-Mora, J. Aragó, J. Calbo, J. Perles, A. Serrano, A. Molina-Ontoria, E. Ortí, N. Martín, M. K. Nazeeruddin, *Adv. Funct. Mater.* **2018**, *28*, 1801734.
[44] "CAM-B3LYP, M06-2X, and wB97X-D functionals were also tested to calculate the excited singlet states looking for a better agreement with the experimental data. All of them predict a similar red-shift of the lowest-lying S1 state of 0.2–0.3 eV in passing from **TPASe-1** to **TPASe-2** (see Figure S3).
[45] L. A. Illicachi, J. Urieta-Mora, J. Calbo, J. Aragó, C. Igci, I. García-Benito, C. Momblona, B. Insuasty, A. Ortiz, C. Roldán-Carmona, A. Molina-Ontoria, E. Ortí, N. Martín, M. K. Nazeeruddin, *Chem. A Eur. J.* **2020**, *26*, 11039–11047.

Manuscript received: May 11, 2021
Revised manuscript received: June 23, 2021
Accepted manuscript online: June 24, 2021